Journal Pre-proof

Shallow geophysical methods for recognition of holocene sedimentary sequences in the southern coastal plain of the Río de la Plata (Argentina)

J.L. Cavallotto, N. Bonomo, V. Grunhut, P. Zabala Medina, R.A. Violante, L. Onnis, A. Osella

PII: S0895-9811(20)30205-4

DOI: https://doi.org/10.1016/j.jsames.2020.102662

Reference: SAMES 102662

To appear in: *Journal of South American Earth Sciences*

Received Date: 6 April 2020

Revised Date: 19 May 2020

Accepted Date: 24 May 2020

Please cite this article as: Cavallotto, J.L., Bonomo, N., Grunhut, V., Zabala Medina, P., Violante, R.A., Onnis, L., Osella, A., Shallow geophysical methods for recognition of holocene sedimentary sequences in the southern coastal plain of the Río de la Plata (Argentina), *Journal of South American Earth Sciences* (2020), doi: https://doi.org/10.1016/j.jsames.2020.102662.

SHALLOW GEOPHYSICAL METHODS FOR RECOGNITION OF HOLOCENE SEDIMENTARY SEQUENCES IN THE SOUTHERN COASTAL PLAIN OF THE RÍO DE LA PLATA (ARGENTINA)

Cavallotto, J.L .[(1)], Bonomo, N.[(2)], Grunhut, V.[(3)], Zabala Medina, P.[(2)], Violante, R.A. [(1)] , Onnis, L.[(2)], Osella, A.[(2)]

[(1)] *División Geología y Geofísica Marina, Servicio de Hidrografía Naval, Buenos Aires, Argentina.*

[(2)] *Departamento de Física. Facultad de Ciencias Exactas y Naturales (FCEyN). Universidad de Buenos Aires, Argentina / IFIBA-CONICET.*

[(3)] *Facultad de Ingeniería-Universidad Austral/CONICET, Buenos Aires, Argentina.*

** Corresponding author: jlcavallotto@hidro.gov.ar*

E-mails of the authors:
jlcavallotto@hidro.gov.ar
bonomo@df.uba.ar
vgrunhut@df.uba.ar
pzabalamedina@gmail.com
violante@hidro.gov.ar
onnis.luciano@gmail.com
osella@df.uba.ar

Abstract

New information about the distribution, geometry, structure, extension and facies variations of the uppermost stratigraphic sequences (particularly the Holocene) of the southern coastal plain of the Río de la Plata was obtained by using geophysical methods. This is the first study performed in the region to investigate the shallow stratigraphic characteristics through continuous geophysical surveys. Methods used were georadar (GPR), electrical resistivity tomography (ERT) and seismic surface waves (SSW), complemented with short drillings. Two transects perpendicular to the coastline were selected on the basis of the previous geological knowledge of the region and accessibility. GPR was used in order to obtain a dense sampling of the near subsoil, whereas ERT and SSW were used in parts of the transects for resolving ambiguous trajectories of the detected GPR horizons. The geophysical results were jointly interpreted, and validated and complemented by the information from the drillings. Two major geophysical horizons were identified; the lower one is located between 5 and 2 meters below surface and progressively shallows inland, which represents the late Pleistocene-Holocene boundary; the upper one, located at variable depths of 2 m to 0.70 m below surface, represents the base of the Holocene beach ridges system in the region. They delimit three units, the lower one corresponding to the top of the Pampean deposits, the middle one representing the basal Holocene sandy layer, and the upper one corresponding to the beach ridges systems and related inter-ridge, tidal deposits. In this way, the applied methodology allowed to determine the extension of the Holocene sedimentary sequences, the relation between the Holocene sequences and its substratum, and the spatial distribution and geometrical characteristics of partially buried beach ridges and associated inter-ridges deposits**.** The applied methodology and the obtained geophysical-response patterns can be useful for future investigations of other regions with similar ground characteristics.

Keywords: Río de la Plata coastal plain; beach ridges; GPR; Geoelectrical method; Seismic Surface Wave method.

1. Introduction

The southern coastal plain of the Río de la Plata, in the province of Buenos Aires, Argentina, is a typical Holocene environment composed of regressive-progradational beach ridges, which contains the records of the last stages of evolution of a large estuarine/fluvial/deltaic environment that constitutes the major geomorphic feature of the region. The surface geology of the coastal plain is known since almost 140 years, and its knowledge has been progressively improved by a considerable number of contributions. However, this knowledge was completely based on surface observations in exposed sections along the margins of rivers, creeks and man-made channels that cut the terrain perpendicular to the coastline, but no continuous geological/geophysical surveys of the subsoil exist up to now, except for few local geophysical surveys focused on specific hydrological or archeological objectives.

Georadar (GPR) is one of the geophysical methods with largest capacity to resolve natural and cultural structures (Paz *et al.*, 2017; Zabala Medina *et al.*, 2020). In geomorphological studies and particularly in coastal regions, the use of this method is acquiring increasing importance worldwide (e.g. Yin *et al.*, 2002; Schortt and Sass, 2008; Van Damm, 2012; Tillmann and Wunderlich, 2012; da Rocha *et al.*, 2013; O´Neal and Dunn, 2015; van Heteren and Fitzgerald, 2017; Dougherty *et al.*, 2019; Leandro *et al.*, 2019). However, most of this research was carried out in open ocean beaches, with some investigations in estuarine shores. In Argentina, the only contribution based on the application of GPR for defining subsurface recent geological structures in a coastal region is that of Colombo *et al.* (2007).

The method has proved to be of high value for geological purposes because it is non-destructive of the subsoil, allows long and continuous records and offers fast and high-quality data. The standard mode of the method is based on the detection of electromagnetic pulses that reflect at interfaces between media with different propagation velocities In particular, the constant-offset antennae configuration is the most popular of the acquisition modes, since it allows acquiring data relatively quickly, although the maximum depth of penetration that can be attained is lower than in other GPR modes, as well as other geophysical methods. The geoelectrical method measures the resistivity of the subsoil (de la Vega *et al.*, 2012; Pipan *et al.*, 2017). It has good resolution and penetration capacities, for a wide variety of environments, although the acquisition of its data is slower than in GPR. The dispersion relation of seismic surface waves, on the other hand, is sensitive to variations in the shear-wave velocity (VS). Therefore, the experimental determination of the group or phase-velocity dispersion curves, followed by a suitable inversion scheme, is a cost effective and nondestructive way to obtain reliable estimates of the shallow VS structure (Schwenk *et al.*, 2016;

Onnis *et al.*, 2019). Each of these methods have the potential of distinguishing facies and sedimentary units characterized by different values of physical properties. Since the three methods respond to different physical properties, they can be jointly applied to increase the probability of detection and the confidence of the resulting interpretation.

The present contribution attempts to begin filling the gap that represents the discontinuous knowledge of the distribution of subsurface units of the southern coastal plain of the Río de la Plata, its detailed geometry, structure, extension and facies changes. Some of those units are of substantial importance as reservoirs of fresh water, deposits of calcareous for mining exploitations and sources of archeological remains, which also shows the importance of surveying them at local and regional scales. Then, in this article we study for the first time details of these structures in a continuous way by using geophysical methods. This includes defining a methodology that describes the structures adequately, which constitutes a secondary objective of the work. To achieve these goals, we define survey lines across the ridge systems and associated environments along which we acquired GPR data. Additionally, geoelectrical and seismic data were acquired at positions of the survey lines in which only approximate interpretations of the subsoil could be obtained from GPR, due to insufficient definition or continuity of the reflections in the radargrams. The geophysical results are validated and complemented with the information from short drillings. After explaining this methodology and its results, an integrated interpretation of the geophysical and drilling information is performed in terms of geophysical/geological units.

2. Working area

The surveyed area (Fig. 1) is located in one of the coastal sectors where the late Holocene beach ridges environments are best represented and well known (in the so call “low terrace”), composed of different ridges systems and associated tidal flats. There, the Holocene sedimentary sequence develops with a thickness of less than 6 m, which has been determined from drillings and outcrops in previous works (Fidalgo *et al.*, 1973 a and b; Cavallotto, 1996, 2002; Cavallotto and Violante, 2005; Fucks *et al.*, 2010; Ricchiano *et al.*, 2012). In addition, another objective of the prospecting was to define the base of the Holocene sequence and the transition to the pre-Holocene substratum. Two representative sub-sectors of the plain, located approximately 40 km apart each other, were selected to perform the studies: Punta Blanca (PB) and Estancia el Destino (ED) (Figs. 1b and 2a). These areas constitute almost the unique sites in this part of the region that provide relatively easy vehicle accessibility, transitable paths for the geophysical systems through the plain, and minor anthropic influence.

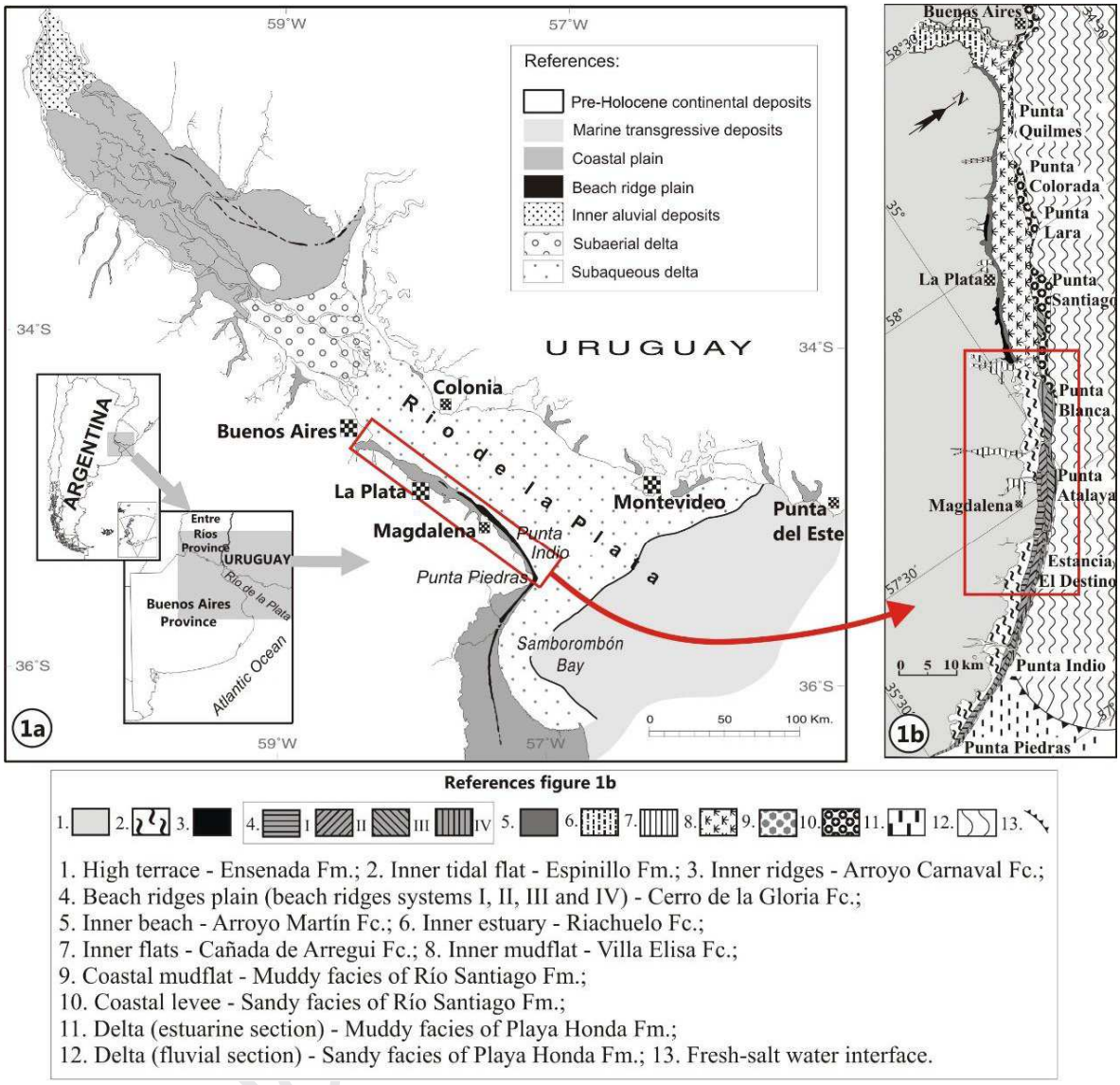

References figure 1b

1. High terrace - Ensenada Fm.; 2. Inner tidal flat - Espinillo Fm.; 3. Inner ridges - Arroyo Carnaval Fc.;
4. Beach ridges plain (beach ridges systems I, II, III and IV) - Cerro de la Gloria Fc.;
5. Inner beach - Arroyo Martín Fc.; 6. Inner estuary - Riachuelo Fc.;
7. Inner flats - Cañada de Arregui Fc.; 8. Inner mudflat - Villa Elisa Fc.;
9. Coastal mudflat - Muddy facies of Río Santiago Fm.;
10. Coastal levee - Sandy facies of Río Santiago Fm.;
11. Delta (estuarine section) - Muddy facies of Playa Honda Fm.;
12. Delta (fluvial section) - Sandy facies of Playa Honda Fm.; 13. Fresh-salt water interface.

Figure 1. Location map. a) Regional map of the Río de la Plata and associated geomorphological environments. b) Map of the sector that includes the studied area.

A field survey for recognizing surface geological units and characteristics of the terrain was initially carried out with the objective of defining the best places to perform the geophysical measurements. This survey revealed that in the PB area –originally selected as the beach ridges plain and associated environments were almost completely preserved there according to the pioneer literature (Cavallotto, 1996, 2002)- coastal retreat due to increasing strong erosive processes as well as partial flooding of the coastal areas have occurred in recent years, what almost entirely erased the beach ridges records. Therefore, in this area it was only possible to access to the innermost environments. Consequently, in order to survey the outermost parts of the beach ridges plain we had to move to the ED section, which provided a more complete development of the ridge´s systems. There we acquired GPR data, whose results were validated and complemented with the execution of very short drillings (up to around 2 to 3 m depth) aimed at obtaining lithological data of the subsoil.

Since the ED section became inaccessible at its landward side (inner tidal flat), we moved back to the PB section in order to complete the survey of that environment, which is well represented in this section. Here, the GPR method was useful in a more limited way due to characteristics of the subsoil and the interference of clutter in the radargrams as a consequence of reflections produced by an electric powerline that runs along the road, as well as the vegetation. To overcome these limitations, the survey was complemented with geoelectrical and seismic surface wave methods.

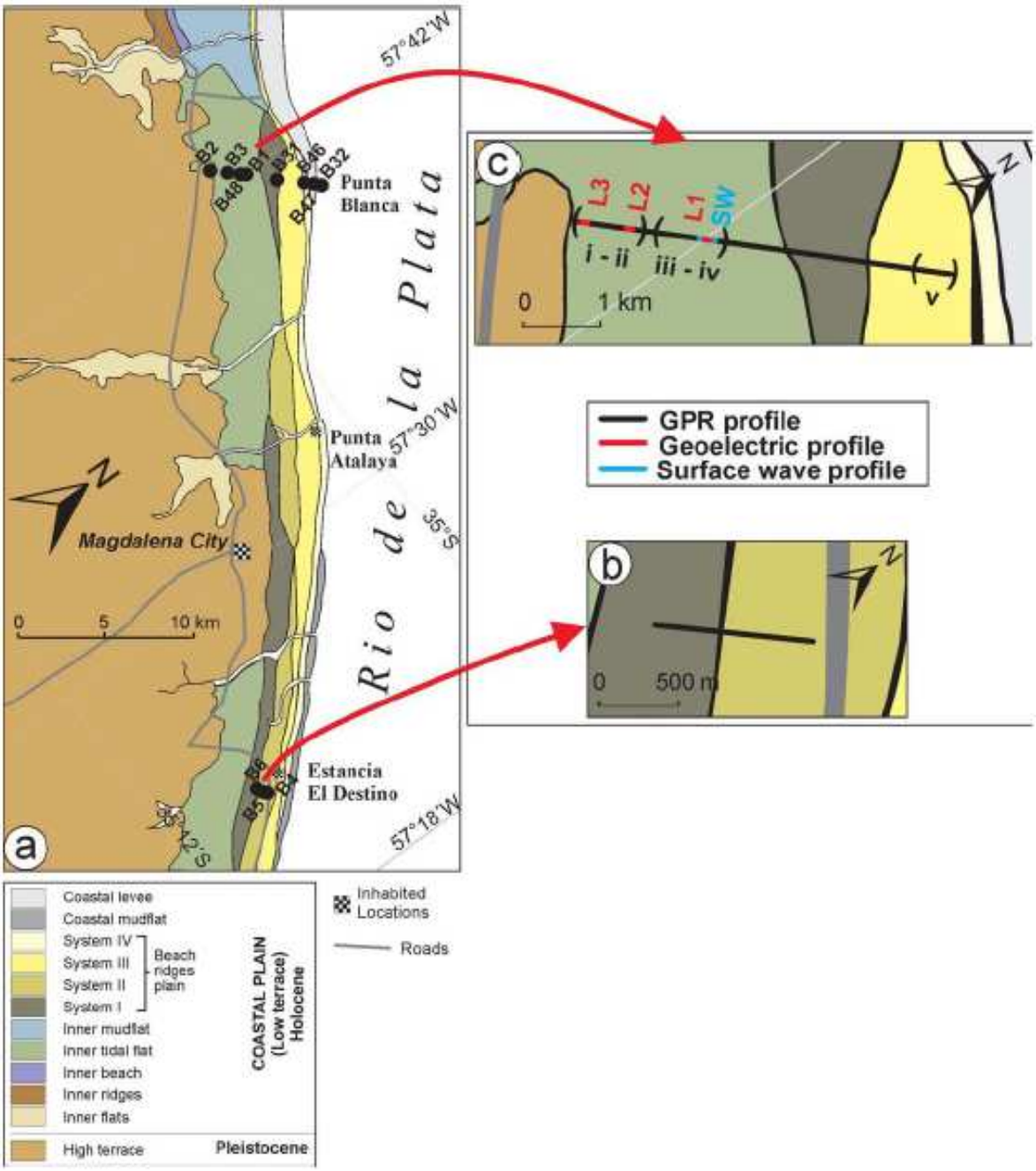

Figure 2. a) Geological map of the studied area and location of the surveyed transects. b) Zoom view showing the location of the GPR profile at Estancia El Destino (ED). b) Zoom view showing the location of the GPR profile at Punta Blanca (PB), together with the geoelectrical and seismic surface wave profiles; (i-ii), (iii-iv) and (v) indicate the sections where GPR data provided clear results.

3. Geological and geophysical background

The regional stratigraphy of the late Pleistocene and Holocene in the southern coastal plain of the Río de la Plata was originally established during the last decades of the XIX century and beginnings of the XX century (pioneer contributions by Ameghino 1880, 1908; Doering 1882, among many others), when the major geological units and stratigraphic relations were originally set based on both surface and outcrops studies as well as on excavations -particularly in large cities as Buenos Aires and La Plata- for constructing buildings, metro lines and ports. Later on, based on the same sources of information, Frenguelli (1950, 1957) significantly improved the stratigraphic scheme (although still informally), which -with little variations and more details in different regions based on contributions of different authors synthesized in Cavallotto, 1996 , 2002; Cavallotto and Violante, 2005- prevailed up to the present. The first local and formal litostratigraphic scheme was done by Fidalgo *et al.* (1973 a and b), later improved by the same authors and colleagues (Fidalgo *et al.*, 1975). In all cases, only surface and accessible subsurface observations were used. After that, Parker and Violante (1993) applied, for the first time, an allostratigraphic scheme (based on Fidalgo´s nomenclature) which was more useful for defining Holocene paleoenvironments and its evolution than the previous ones. That scheme was particularly improved and definitively established in the region by Cavallotto (1995, 1996, 2002), Cavallotto *et al.* (2004) and Cavallotto and Violante (2005), based not only on surface geology but also by performing deeper drillings up to around 30 m depth, and using for the first time available bibliographic information (basically sedimentological) coming from old water and geotechnical drillings up to several tens or a few hundreds of meters depth. In more recent years, Fucks *et al.* (2010) and Richiano *et al.* (2012) made minor changes in the stratigraphic scheme.

Some bibliographic background exists about geophysical studies in specific locations of the region. Geoelectrical surveys using the Schlumberger electrode configuration have been successfully performed as a complementary technique for deriving hydraulic parameters of deep aquifers in the city of La Plata (Perdomo *et al.* 2014). More recently, a 2D resistivity survey based on a combination of different configurations was implemented by Perdomo *et al.* (2018) in order to identify the complexity of the alluvial sediments at a range of 30–70 m deep, quantifying the 2D variation of hydraulic parameters in the semi-confined aquifer “Puelches” in La Plata. On the other hand, Cellone *et al.* (2018) established an electrostratigraphic model in a sector of the coastal plain close to Punta Indio and produced an electric conductivity map of the near surface aquifer. Colombo *et al.* (2007) used GPR to obtain images of the internal structure of Holocene sequences in the Paraná delta.

However, the presently known stratigraphy is not based on continuous (either local or regional) subsurface observations. This is the main objective of the present work, in which we

construct the first long continuous section of the near-surface geological structure based on geophysical surveys.

4. Regional geomorphology

The Río de la Plata is a large funnel-like fluvial-estuarine environment open to the southwestern Atlantic Ocean, which is around 300 km long and has a width of few kilometers at the estuary head and 220 km at the outlet to the sea. This environment is believed to have been formed at around 2.4 My and was affected by all the Quaternary sea-level fluctuations that left different geological records in the subsoil in both the underwater and the coastal regions (Parker *et al.* 1994). The postglacial marine transgression that followed the Late Glacial Maximum (LGM) and the subsequent late Holocene regression started after 6000 yr. BP, conditioned the present-day characteristics of the region, by modeling both the subaqueous and the coastal environments, with a final evolution in the last 2000 years given by the development of the delta environment that progressively invaded the estuary (Cavallotto *et al.* 2005). In the southern coast (that includes the presently studying area) an extensive coastal plain was formed.

The Río de la Plata southern coastal plain is made up of regressive late Holocene sedimentary sequences, extended from the river shoreline to the innermost inland boundary approximately coincident with the countourline of +5/6 meters a.s.l. The coastal plain constitutes, morphologically, a relatively flat surface call “low terrace” with an altitude gradually decreasing towards the river from 5 m a.s.l. to 0 m. At its innermost boundary a 1 to 2 meters high step separates that surface from another relatively flat surface located above 6 m a.s.l., which is call “high terrace”, a feature whose substrate is composed of pre-Holocene continental deposits (“Pampean beds”) and was never reached by the last transgression.

The southern coastal plain extends alongshore for more than 300 km. It is composed of a large set of regressive facies evolved during the sea-level fall that followed the last sea-level highstand, which occurred at around 6000 yr. BP (Cavallotto 2002, Cavallotto *et al.* 2004, Cavallotto and Violante 2005, Prieto *et al.* 2016). The entire set of present- and paleo-environments includes several systems of beach ridges, low-energy beaches, tidal flats, mudflats, and coastal levees (Fig. 1). In the study area (Fig. 2a) three major geomorphic features shape the coastal plain: beach ridges plain, inner tidal flat and coastal mudflat.

4.1. Beach ridges plain

It is the most conspicuous feature of the region extending for more than 200 km. It is composed of four sets of ridges at decreasing topographic levels towards the river coastline, from 5 to 2.5 m above sea-level (Cavallotto 2002, Cavallotto *et al.* 2004). Erosive unconformities separate each set of ridges, revealing that during the sea-level fall intense erosive processes with a slight coastal retreat (probably associated to momentaneous stabilizations of the sea-level) took place at the end of deposition of each set before the development of the next set at a lower-than-the-precedent level. Each set is made up of a numerous of individual ridges that correspond to beach deposits associated to littoral bars, composed of bioclastic sediments with subordinated amounts of sand, which locally becomes dominant. The ridges located in areas closer to the shore are almost exclusively sandy. Inter-ridges deposits are composed of sandy to clayey silts, which correspond to protected back-bars, low-energy environments. Malacological and microfaunistic associations indicate for these deposits paleoenvironmental conditions related to an open estuary with temperature and salinity higher than the present-day conditions in the area (e.g. Aguirre 1993, Aguirre and Whatley 1995).

During the surveys carried out for the present study, we noted that in PB most of the ridges previously described in the 80´s and early 90´s (Cavallotto, 1995) do not longer exist nowadays due to coastal erosion and shoreline retreat, a common recent process along different places of the southern coastal plain of the Río de la Plata. According to the descriptions by Cavallotto (1995), the today not existing ridges were of low topographic expression and recognized in the field by the straight lines of vegetation that covered them (particularly *celtis tala*, a tree species that grows on permeable, calcareous substrata such as that typical of the ridges). Instead, in ED the ridges are preserved as they extend further inland from the shoreline and are protected from coastal erosion by the presence of a coastal mudflat.

4.2. *Inner tidal flat*

It extends inland from the innermost beach ridges as a low-lying, slightly depressed area that represents the tidal environment developed behind the beach ridges during the last highstand. This environment extends up to the border of the “high terrace” that marks the maximum reach of the Holocene transgression. It is composed of clayey sands containing a typical faunal assemblage indicating littoral mixohaline conditions (Cavallotto 2002).

4.3. *Mudflat*

This is a narrow strip of coast that separates the beach ridges plain from the present shoreline, and therefore represents the sector flooded during extraordinary high tides where muddy sediments from the Río de la Plata containing estuarine faunal associations are deposited.

5. Methodology

Based on the previously known geology and geomorphology of the region (Cavallotto 1995, 2002, Cavallotto *et al.* 2004), geological surveys at the Estancia el Destino and Punta Blanca areas (see Fig. 2) were performed before selecting the locations for the geophysical surveys and drillings.

5.1. Short drillings

Short drillings up to 3 m depth were performed at specific locations along the ED and PB transects using a handly-operated rotating system, which consisted of a 0.3 m long and 2 inches wide helical bore placed at the bottom of a set of metallic bars. Sediment samples were obtained at variable depths between 0.1 m and 0.3 m as the drilling progressed. The samples were described *in situ* in order to define sedimentological characteristics useful for stratigraphic determinations and correlations. Since sedimentological information from previous short drillings already existed in the region (Cavallotto 1995), the locations of the new drillings were set with the objective of filling gaps in the sectors to be surveyed by geophysical methods. The drillings allowed to recognize six lithological types, named I to VI (described in the Results section of this paper).

5.2. Geophysical surveys

The ability of the GPR method to quickly investigate the subsoil in detail was used to extensively record the geological structure along selected transects. At ED, a 1 km long GPR profile was acquired. At PB, a 5.1 km GPR profile was surveyed, complemented with electrical resistivity and seismic profiles in places were the GPR method produced unclear results. The location of the geophysical profiles is indicated in Figure 2b; in each area, the x-coordinate system begins at the west end of the survey line and increases towards the coast. GPS Ashtech Promark 2 was used for precise location of the geophysical measurements and drillings in the field (see Fig. 2b).

GPR prospecting: the GPR data were acquired with a pulseEkko Pro system. Two pairs of antennae, with nominal frequencies of 250 MHz and 100 MHz were employed, in standard constant-offset

reflection mode (Jol, 2009). These frequencies provide different resolution of the layers and penetration of the electromagnetic waves in the ground. In general, higher frequencies produce a better resolution of the layers, whereas lower frequencies increase the depth of penetration. The 250 MHz antennae were mounted on a skid plate, whereas the 100 MHz antennae were supported by a cart. The offset between the antennae was 0.4 and 1 m, respectively. An odometer wheel triggered the acquisition of traces at a regular spacing of 0.04 and 0.2 m, respectively. The time window was set to 200 and 300 ns, and the time increment to 0.4 and 0.8 ns, the system default values. The number of stacking at each sampling position was 16.

The data were processed by applying a sequence of standard GPR procedures programmed in Matlab code (Bonomo *et al.*, 2011; 2012). Firstly, a high-pass time filter was applied inside a sliding window to remove low-frequency induction effects of the antennae, commonly known as "wow". The size of the time window was three periods. Then, fluctuations of the default time-zero reference of the traces were compensated with respect to the mean value of this parameter. A high-pass spatial filter was used to remove the direct waves (cut frequency at 0.01 1/m), and a mean-amplitude gain curve was applied to compensate wave attenuation. A mean velocity of propagation of the waves in the subsoil was obtained in each investigated area by fitting hyperbolae to the diffractions in the data sections and by averaging the results. This velocity was used to convert the time scale to depth.

Figures 3a and 4a show the processed GPR profiles obtained in ED with the 250 and 100 MHz antennae, respectively. In this sector, several reflectors are visible, whose continuity can be established with precision, as those indicated in Figures 3b and 4b, respectively. With the 250 Mhz antennae a good detail of the most superficial layers, up to 1.9 m depth (48 ns) is obtained, while the 100 Mhz antennae provide information down to a depth of 5.3 m (130 ns), approximately. The mean propagation velocity obtained in this sector is 0.081+/-0.015 m/ns. Two main reflectors are observed in the profiles: the shallowest one is located at a depth between 0.6 m and 1.8 m (30-90 ns, thick red line in Fig. 3.a), whereas the second one is located between 2.7 m and 3.7 m (135–185 ns, thick green line in Fig. 4.a). Several noticeable diffractions are visible throughout the 100 MHz radargram (Fig. 4a), such as those between 580–640 m and 50–135 ns. They are air reflections, as deduced from velocity analysis performed on them, and are produced by the presence of vegetation near the survey line, since these antennae are not shielded. On the contrary, the 250 MHz profile (Fig. 3.a) doesn´t show this type of reflections, because in this case the antennae are shielded. Finally, a number of reflectors are observed in the 100 MHz profile below the lower main reflector (Fig. 4), which are approximately parallel to it. They are part of the internal structure of the lowest detected layer.

In the PB sector, on the other hand, the subsoil conditions were different than in ED and the ground showed a higher content of moisture in surface. This diminished the amplitude of the GPR waves with the highest frequencies. As the data were acquired on a dirt road, the continuity of the shallowest horizons seemed to be destroyed due to the movement produced by the vehicular traffic and the road consolidation works. As a consequence, the 250 MHz profiles did not provide relevant information on the shallowest part of the subsoil (not shown). On the contrary, the 100 MHz profiles (Fig. 5) show several reflections after the direct waves (below 1.65 m, 32 ns, approximately), with different sharpness and continuity depending on the position along the profile. The mean velocity of propagation in this sector is 0.104 +/-0.006 m/ns. The average penetration depth is around 5.2 m (100 ns). Since the 100 MHz antennae were not shielded and the amplitudes of the subsoil reflections were low, many reflections produced by objects located in air (trees and a nearby power line) prevailed over the first ones in different x-t intervals and masked them partially or completely. Figures 5a i to v are examples of different sections of the profile. Prominent reflections are observed between x = 0 m and 4540 m and 70 ns and 110 ns (Figs. 5a i to iv), which are generated by the cables of the power line. Equally spaced diffractors are observed near the cable reflections (e.g., at x = 355 m, 415 m, 475 m, etc. and t = 92 ns in Fig. 5.a.i), which are associated to their supporting posts. The signals of the surface vegetation can be observed in different parts of the profile as isolated hyperbolae (e.g., x = 435m, t = 60 ns in Fig. 5.a.i) or densely packed groups of hyperbolae (e.g., x = [490 – 530] m, t = [35 – 70 ns] in Fig. 5.a.i). Despite these types of reflections, two other types of relevant reflectors can be identified in the profile. The first one is related to a reflector that appears just below the direct waves at x = 580 m, and that deepens towards the end of the profile (thick green lines in Fig. 5.a). The depth of this reflector is 1.7 – 2.6 m (32 - 50 ns) in Fig. 5.a.i, and 3.9 - 5.2 m (75 - 100 ns) in Fig. 5.a.v. In different sections of the profile, the continuity of the reflector is unclear due to its low reflection amplitude with respect to the clutter and noise (e.g., in the x-interval 1920–2130 m of Fig. 5.a.iv) or the presence of irregular and nearby reflectors with similar inclinations (e.g., in the x-intervals 840–1100 m of Fig. 5.a.ii), whereas in other sections the continuity is fairly good (e.g., in Fig. 5.a.iii). Due to the limited definition of the method in the time interval occupied by the direct waves, only a tentative trajectory of the reflector could be established for x < 560 m (Fig. 5.a.i) in the sector where it gets very close to the surface and crops out according to nearby surface observations. The second type of reflectors are represented by relatively inclined and irregular interfaces that extend below, from the lower limit of the direct waves to the previous reflector, which deepens towards the coast (e.g., Fig. 5.a.v, thick red lines). These reflectors are visible from x = 2900 m to the end of the profile.

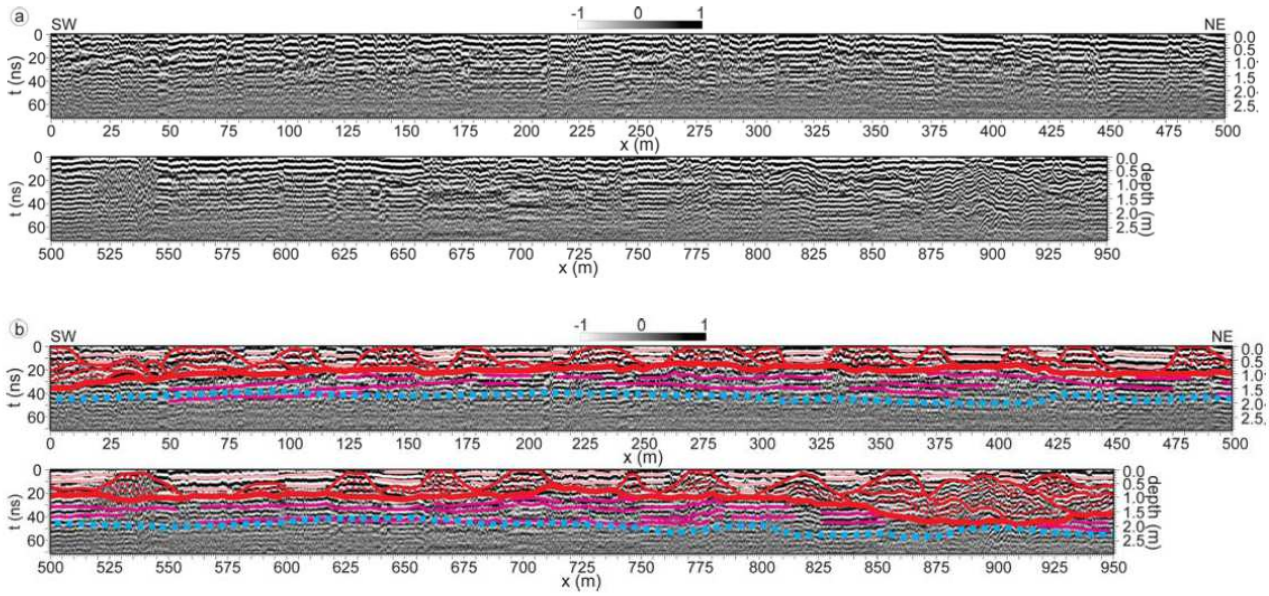

Figure 3. GPR section of Estancia El Destino, obtained with 250MHz antennae. a) Processed data; b) Relevant reflection horizons indicated in different colours.

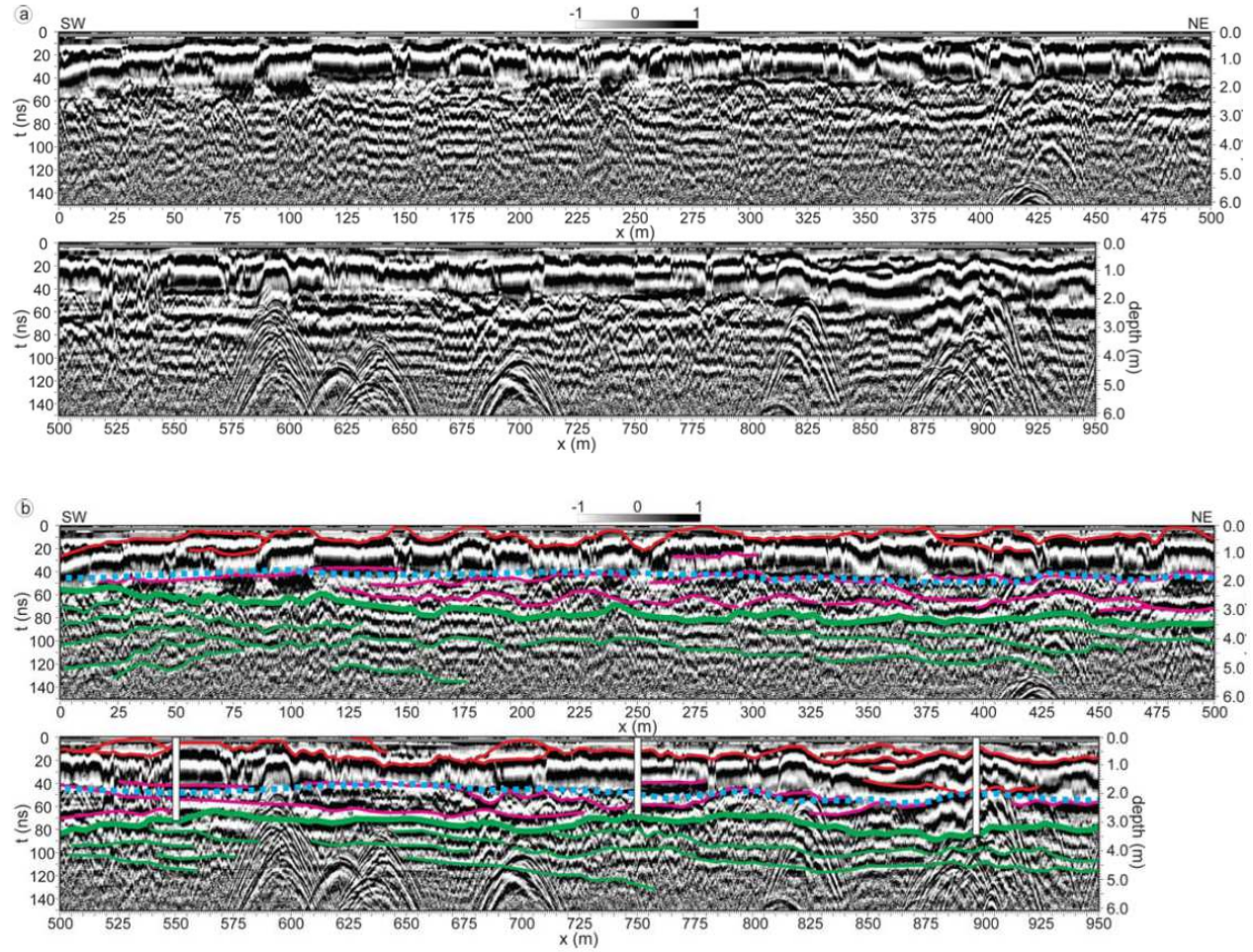

Figure 4. GPR section of Estancia El Destino, obtained with 100 MHz antennae. a) Processed data; b) Relevant reflection horizons indicated in different colours.

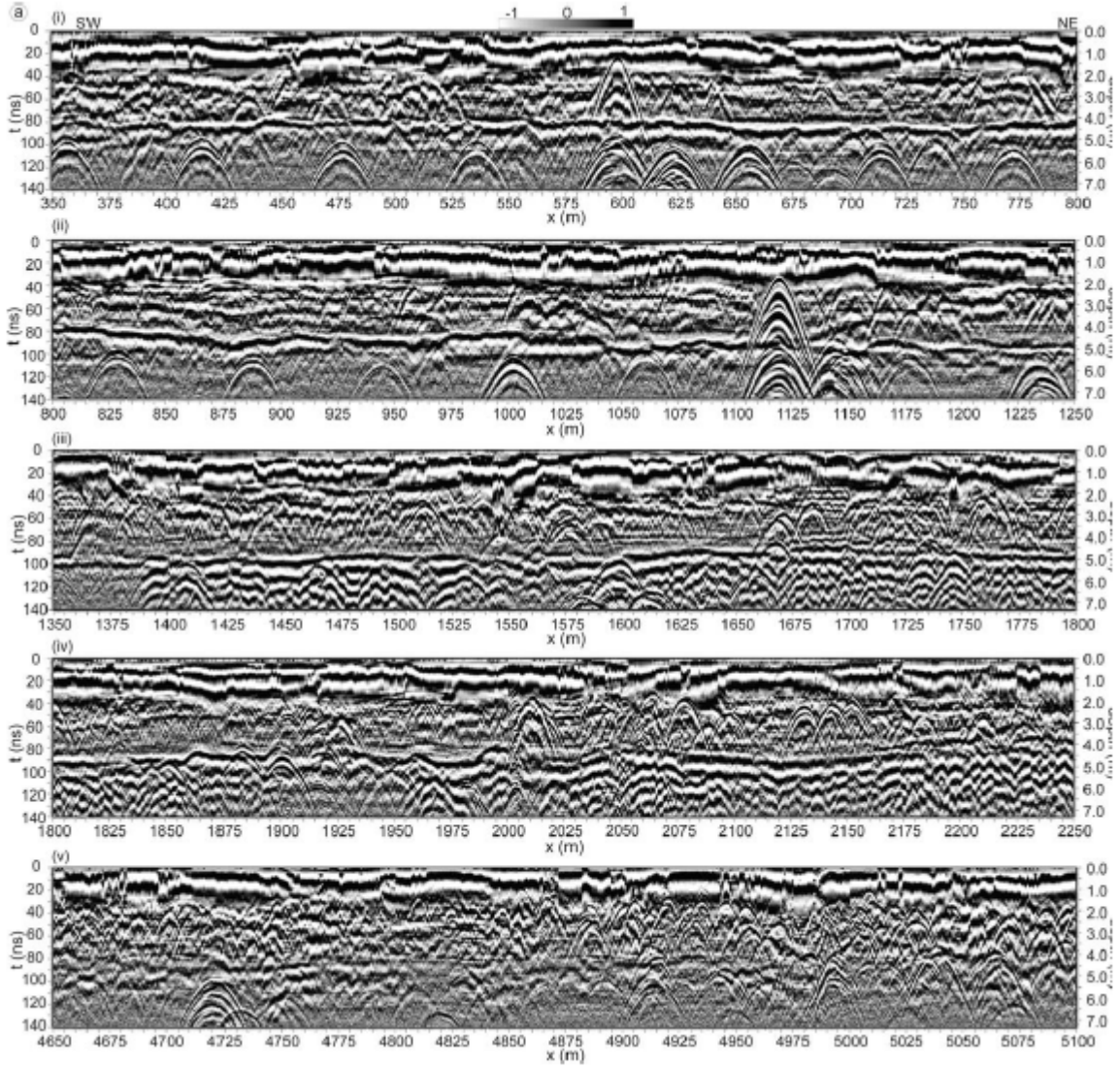
a
(i) SW
NE
-1
0
1
t (ns)
x (m)
(ii)
(iii)
(iv)
(v)

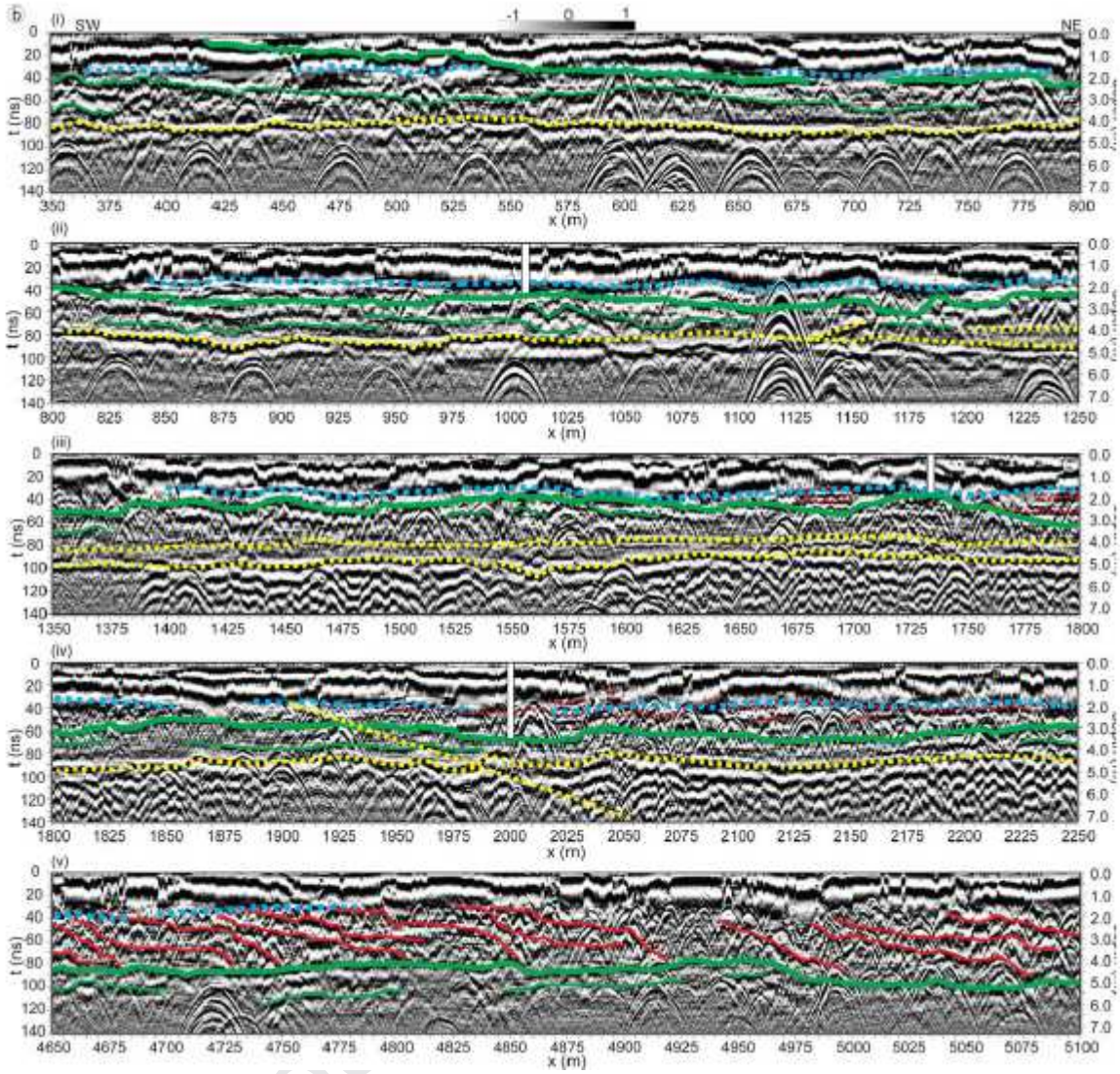

Figure 5. Different sections (i to v) of the GPR profile obtained in Punta Blanca with 100 MHz antennae, as shown in Figure 2b. a) Processed data; b) Yellow dotted lines correspond to electric power cables. Other colours indicate reflections in discontinuities of the subsoil. Vertical bars show the location of drillings.

Geoelectrical prospecting: To complement the interpretation of the GPR data in ambiguous sections of the PB transect, geoelectrical profiles were performed. A first geoelectrical profile was located at 2000 m from the origin, where the GPR reflectors were unclear and a short drilling was already available; the other profiles were centered at 1000 m and 400 m, respectively (see Fig. 2c). In the first of these positions, GPR showed unclear trajectories of the reflectors, whereas the last position agreed with the zone estimated for the outcropping of one of the main reflectors.

Data were acquired using Saris 250 equipment (Scintrex). Concerning the electrode configuration, several studies that compare the advantages and limitations of different arrays (Dahlin and Zhou 2004, Martorana *et al.* 2009, Szalai *et al.* 2011) revealed that the dipole–dipole

configuration can provide a comparatively good penetration depth and one of the best imaging resolutions. On this basis, we decided to use the dipole–dipole configuration for this study.

It is known that the electrode spacing influences the maximum penetration depth. Taking into account the expected characteristics of the subsoil, electrode spacings dx = 1.5 m, 3 m and 4.5 m were selected, with dipole separation factors, n, up to n = 6. In this way, it is possible to increase the depth of penetration keeping the lateral resolution approximately constant. All the profiles have a length of 58.5 m, with a maximum investigation depth of approximately 12 m, which was enough for the objectives of this work.

To obtain the electrical resitivity tomographies, the data were inverted using the RES2DINV software, version 4.06.12 (developed by Loke and Barker 1996). For each profile, the data acquired with all the electrode spacings were inverted together to improve both the resolution and penetration depth of the resulting models. We selected the usual least-squares (L2 norm) inversion for all the profiles because it generates models with smooth resistivity variations (DeGroot-Hedlin and Constable 1990) that are more consistent with the resistivity structure expected for the site than sharp variations. The mesh was refined to four nodes between adjacent electrodes in order to improve the results by minimizing the errors. The models were accepted within 5 iterations after the absolute error no longer significantly changed (with 2% default error tolerance).

The resulting ERTs are shown in Figure 6. In Line 1 (Fig 6.a; obtained with RMS = 3.6%), which corresponds to the x-position 2000 m, it can be observed two main resistivity zones and a transition zone between them: a more conductive shallow zone, which occupies the depth interval from the surface to 1.9 m approximately, a more resistive zone below 3.0 m approximately, and the transition zone that includes a series of relatively low resistivity anomalies located in the x-interval 23-46 m. Regarding Line 2 (Fig 6.b; obtained with RMS = 3.6% too), which corresponds to the central x-position 1000 m, the shallow conductive layer has a lower limit at a depth of 1.8 m approximately, in the x-interval 0–17 m, whereas in the rest of the profile this layer is compressed downwards by a series of very shallow resistive anomalies. In this tomography, the resistive layer is located below a depth of 2.6 m. The dotted and solid lines marked in Figures 6a and b, indicate the approximate bottom and top boundaries of the high and low resistivity zones mentioned above, respectively. The depths of these boundaries are coincident with the horizons obtained with GPR (dotted blue and green lines of Fig. 5, respectively). On the other hand, in Line 3 (Fig. 6c; obtained with RMS = 2.3%), which corresponds to the x-position 400 m, the conductive layer is absent while the underlying resistive medium appears just below the surface. This result indicates that the outcrop position of the layer is located between the end of this profile and x= 560 m, where the correspondent GPR horizon is lost due to the presence the direct waves along the surface.

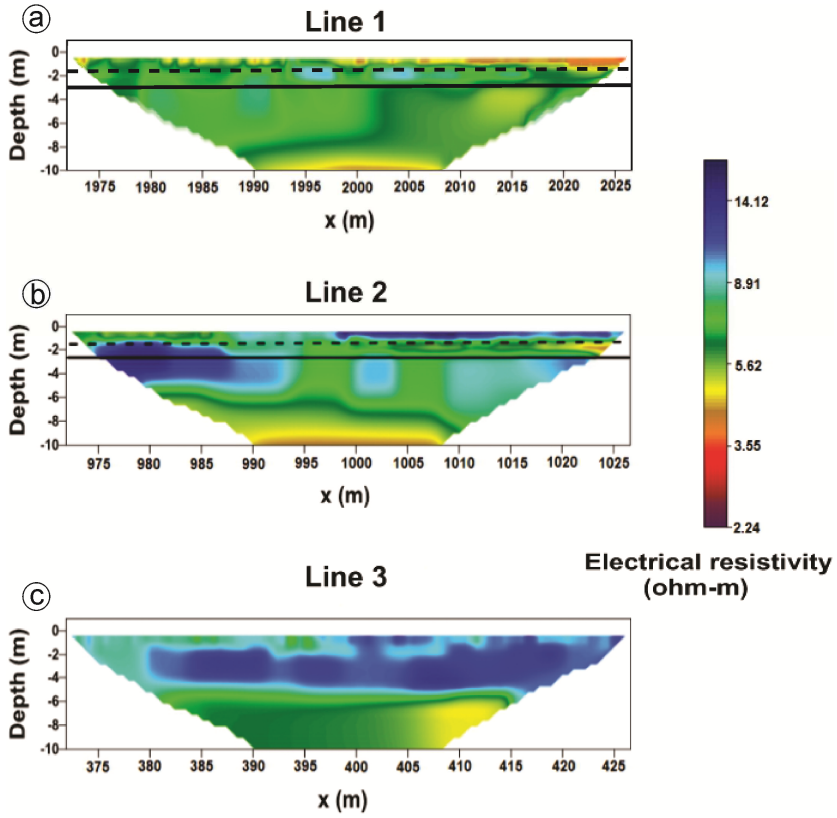

Figure 6. Electrical resistivity tomographies obtained in Punta Blanca, at (a) x = 2000 m, Line 1, (b) x = 1000 m, Line 2 and (c) x= 400 m, Line 3, respectively. Dotted and solid lines indicate the lower boundary of a relatively high resistivity layer and the top of a lower resistivity zone, respectively, which coincides with the dotted-light-blue and solid-green lines in Fig. 5b.

Seismic surface wave analysis: the seismic profile was surveyed at the PB section, with center at 2000 m, so it was coincident with the GPR profile, one of the geoelectrical profiles and one of the drillings. A MASW (Multichannel Analysis of Surface Waves) survey was performed along a 230 m line (see Fig. 2c). The acquisition was carried out using a Geometrics Geode DZ system, 96 receivers with 2.5 m separation (10 Hz vertical geophones), and a 1000 Hz sampling rate. A 3.0 s recording time-window was selected to allow the slowest surface waves (~ 100 m/s) to reach all receivers within the acquisition window. The source, a 10 kg sledgehammer operated manually was activated two times at the midpoint of each consecutive receiver pair (every 2.5 m).

A 2D shear-wave velocity section was derived following the methodology widely detailed in Onnis *et al.* (2019). As it is not a commonly used methodology for this type of studies, a brief summary is given here. The surface wave analysis of the line consisted of three steps. In the first step the seismic line was divided into overlapping receiver segments, 50 m long each, and the shots for the analysis of each segment were identified. The partitioning of the line in several segments is

intended to make the hypothesis of 1D inversion plausible, and at the same time to allow the retrieval of lateral variations along the line.

In the second step, a representative f-k amplitude spectrum was computed for each segment by averaging the f-k amplitude spectra of several shots. The f-k domain was chosen to pick the phase-velocity dispersion curves due to the presence of noticeably aliased components. The implemented stacking strategy significantly improves the SNR (signal-to-noise ratio) of the surface waves, and results in smooth, interpretable f-k spectra in which modal curves could be identified. In this case, a single phase-velocity dispersion curve, which corresponds to the Rayleigh fundamental mode was picked for each average spectrum. Additional signals were observed but not adequately resolved to enable picking.

Finally, the picked curves were inverted by means of a 1D global optimization method, the Neighborhood Algorithm (Sambridge 1999), as implemented in the Dinver open-source package (Wathelet *et al.*, 2004; Wathelet, 2008). This method consists of searching for a model (within a given parameter space) that minimizes the misfit function, defined as the RMS-error-weighted discrepancy between the modeled and target phase-slowness dispersion curves. Forward modeling is done by following Dunkin (1965). The complete procedure is described in Onnis *et al.* (2019). The resulting 1D velocity models were combined in order to obtain 2D pseudosections.

Regarding the parameter space used to perform the analysis, we considered a search space composed of 1D layered models. Each model was initially characterized by a single density value, common to all layers, which was allowed to vary between 0.8 kg/dm^3 and 3.0 kg/dm^3. Values for the acoustic and shear-wave velocities were restricted to the 150-5000 m/s and 100-3250 m/s intervals, respectively. In order to prevent the allowed layer geometry from biasing the results, different geometries were analyzed following Cox and Teague (2016), with 5 layering ratios ranging from 1.2 to 2.0. This yields models with 4 to 7 layers (including the underlying half-space). The top of the lower half-space was limited to a maximum depth of 13.5 m. Additionally, Poisson's ratio was constrained between 0.45 and 0.5 beneath the water table (Bishop and Hight, 1977).

Each inversion sampled 100.000 models. Inversions with a layering ratio of 1.6 (5 layers) produced the lowest average misfit along the line. There were no significant differences between the results yielded by the different employed parameterization strategies. Figure 7 shows the shear-wave velocity results for each inverted curve using the parameters mentioned above, with the center coordinate of the corresponding segment indicated. These results show a smooth lateral variation and a consistent increase of shear-wave velocity with depth. There is a small but consistent jump in the velocity at a depth of approximately 1.2 m, from 105 m/s to 130 m/s and a more significant increase from 130 m/s to 250-300 m/s at a depth of 3-4.5 m. All these velocity values are consistent with the propagation of Rayleigh waves in fine sediments, with the lower near-surface values

corresponding to unconsolidated clays. The increment in the velocity with depth can correspond to denser, more compacted sediments, and is compatible with both the resistivity transitions observed from the ERT results, and the lower main reflector found from the GPR data.

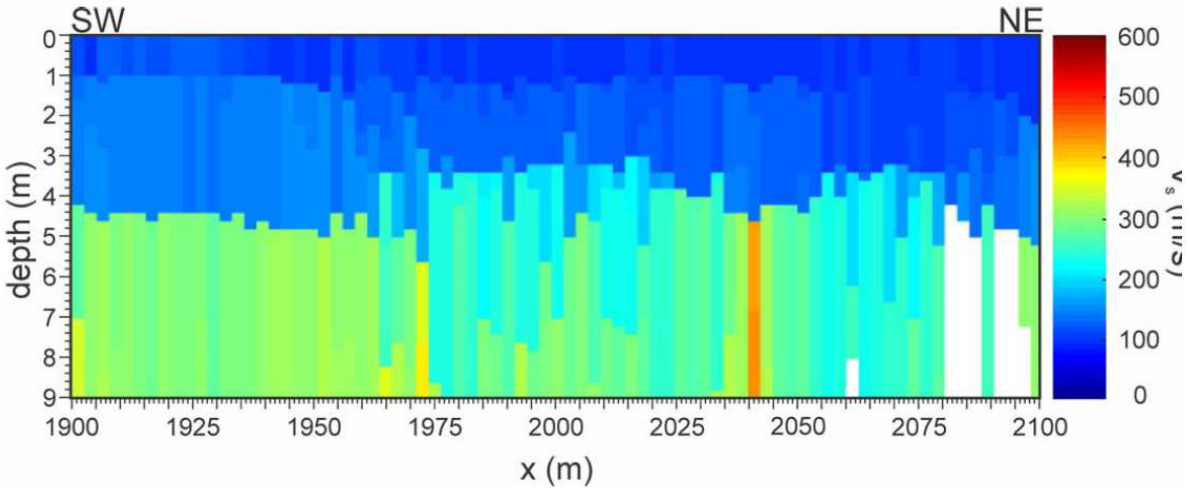

Figure 7. 2D velocity section, V_s, built from the inversion of the 1D dispersion curves, at Punta Blanca (see location in Fig. 2c). White gaps correspond to positions at which inversion resulted unreliable due to excessive dispersion.

6. Interpretation of the results

6.1. *Geophysics*

The integration of the geophysical results of the two studied sections allowed interpreting the investigated near-surface stratigraphic sequences. In Estancia El Destino, the GPR measurements obtained from antennae with different resolutions and penetrations provided detailed information about the uppermost layers, represented by the complete set of beach ridges and its internal structure as well as the inter-ridge areas, as well as the transition from that unit to the underlying substrate. In three sections of the Punta Blanca profile, the GPR results were not as clear and unambiguous as in the ED section so we made tentative interpretations of them. In these sections, we performed complementary geoelectrical and seismic surface waves surveys, whose results confirmed the GPR provisional interpretation of the layer boundaries in two of the problematic sections and also provided additional information about the media that compose the layers. In the remaining ambiguous GPR section, the ERT results moreover confirmed the westernmost termination of the beach ridges units and the outcropping of the underlying substrate. Short drillings carried out in selected places along the PB and ED sections allowed validating and complementing the geophysical interpretation with lithological information.

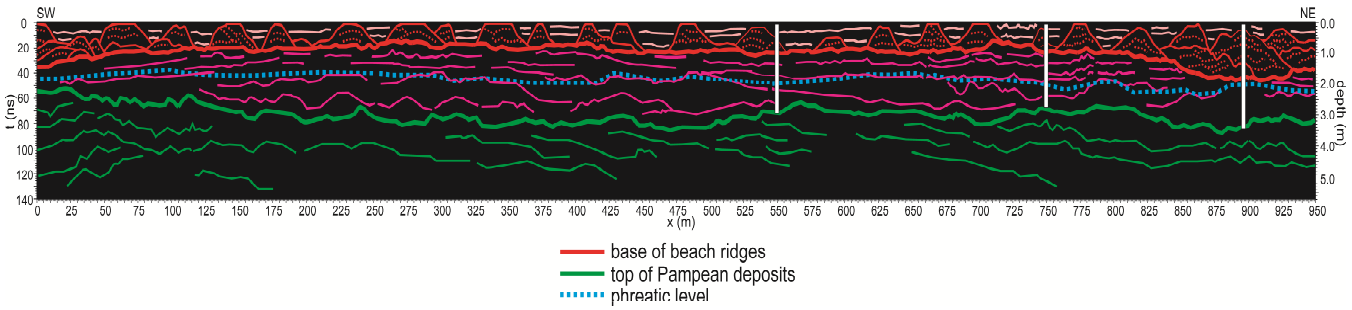

Figure 8. Synthesis of the GPR results at Estancia El Destino, obtained with 250 MHz and 100 Mhz antennae (Figs. 3b and 4b, respectively), and the corresponding interpretations of the stratigraphy. Vertical bars show the location of drillings.

In order to describe the stratigraphy and geophysical/geological units that result from the geophysical prospecting, we consider the scheme of Fig. 8, for the ED section. The uppermost horizon in this section corresponds to the thick red line defined by GPR (shown in Fig. 8), which correlates with the boundary of the shallowest seismic layer with very low velocity defined by surface waves at PB; in the case of the geoelectrical prospecting, an equivalent layer was probably masked by the water table. On the other hand, the deeper horizon corresponds to the green-line horizon defined by GPR (shown in Fig. 8), which correlates with the lower transition boundary of the resistivity method, probably indicating compact sediments, and the line representing the jump in seismic velocity to 250 m/s defined by surface waves.

In the following description, the horizons are named from top to base “a” and “b”, which separate three major units, named from top to base A, B and C. Description are given in stratigraphic order, from base to top (see Fig. 9 for synthesis).

Horizon “b” (thick green line in Fig. 8): it is a relatively irregular surface located at gradually decreasing depths westward. In PB (Fig. 5.b, where it is also indicated by a green line), it reaches a larger maximum depth, in the easternmost part of the profile than in ED (5.2 mm vs. 3.7 m, respectively). Some depressions of this horizon, which probably represent paleochannels, are visible along the ED and PA profiles, as those of the x-intervals 2225-1925 m (Fig. 5.a.iv), 1850-1750 m (Figs. 5.a.iii and iv) and 1225-1075 m (Fig. 5.a.ii). The steep projection of the horizon towards the surface indicates that it crops out at an approximate position 400-500 m (Fig. 5.a.i, dotted line).

Horizon “a” (thick red line in Figure 8): it is not observed in the GPR section of PB due to the lack of information on the first two meters of the subsoil. Instead, in ED it is seen at a variable depth of 0.6–1.8 m with an irregular surface, which shows a trend of decreasing depths westward. At the eastward side it shows a scarp around 0.80 m high.

These horizons determine three geophysical units, described from base to top (Fig. 8):

Unit "C" (below horizon "b", thick green line in Fig. 8): this unit contains discontinuous and aggrading internal horizons, indicating an aggrading depositional pattern. In parts of the GPR record it is evident that horizon b represents an erosional surface as some toplap structures in landward direction are observed.

Unit "B" (between horizons "b" -thick green line- and "a" -thick red line-) (Fig. 8): this unit shows diverse patterns, changing from wavy close to the coast to subhorizontal inland. In the PB section it shows a marked prograding-to-the-coast pattern. The uppermost part of this unit is more aggrading than the lower part. The aquifer water table is contained in this unit.

Unit "A" (above horizon "a", thick red line): In ED it is possible to clearly identify two subunits (Fig. 8). The lower one is a regionally continuous sedimentary package with a nearly regular series of conspicuous mound-like structures resting on horizon "a", composed of large mounds, each of them having an internal mounded structure. The uppermost unit is discontinuous as it develops between the mounds, showing a horizontal, parallel aggrading structure.

6.2. *Lithology*

The short drillings recorded the expected lithologies according to the known stratigraphy and sedimentology of the region. Six lithological units are described (named I to VI from top to base), in most of the cases with transitional and gradual contacts between them, except for the unconformable and relatively sharp contact above the lowermost unit VI. The following description is given in stratigraphic order from base to top:

VI: Compact, greenish to grayish brown silty sediments with calcium carbonate concretions and caliche pebbles. The boundary between this one and the underlying units (that can be V or IV) matches the position of horizon "b".

V: Olive to browned gray silt with limolitic spots.

IV: Loose to semi compacted brown sand (sometimes slightly clayey), containing small grains or even gravelly-sized pieces of calcium carbonate concretions; this unit contains the aquifer level.

III: Loose, fine yellowish brown sand with highly fragmented shells.

II: Shelly sands that characterize the sectors were beach (shell) ridges were drilled, composed of diverse mixtures of fine, light brown and yellow sands with variable amounts of shell fragment (sometimes dominating over the sands); iron oxide specks are common in the lower levels;

I: Soft, water-saturated, sometimes very plastic greenish, olive and browned clay located in the inter-ridges; iron oxide and calcium carbonate concretions are common.

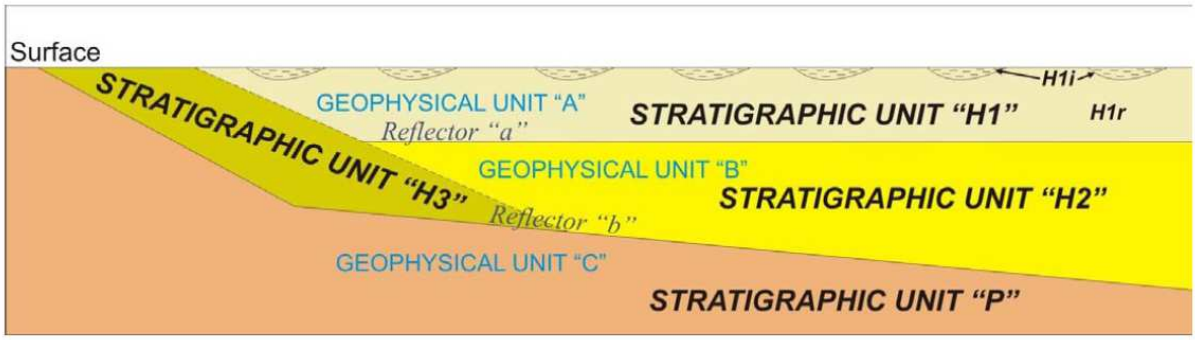

Figure 9. Schematic stratigraphic horizons and units.

7. Definition of geophysical/geological units

Although three units were identified after the application of the used geophysical methods, they correspond to four lithostratigraphic units according to the well-known regional geological scheme (Fig. 9) and the recognized lithologies in the performed short drillings. They are described from bottom to top.

Unit "P": continental (mainly fluvial) deposits that correspond to the Pampean unit (particularly Ensenada Formation of late Pliocene-Pleistocene age), defined in this region by Cavallotto (1995, 1996), which represents the substratum of the Holocene (post-glacial) sequence. This unit was recognized in PB and ED transects, being its top represented by horizon "b", which corresponds to the unconformity separating it from the uppermost (Holocene) units. It is represented by lithological unit VI.

Unit "H3": Deposits that correspond to Espinillo Formation (Cavallotto 1995, 1996) of mid-Holocene age, correlated with the unit that represents the last stage of the Holocene transgression when sea-level reached its maximum position, in transition to the beginning of the regressive event. This unit, that stratigraphically underlies Units H2 and H1, was not clearly identified on the basis of the analyzed geophysical information since no sharp contact was detected separating it from the adjacent units. However, lithological unit V found in one of the drillings fits very well with the sedimentary characteristics of Espinillo Formation in a place where this unit was expected to develop according to previous studies (Cavallotto 1995, 1996). Therefore it is considered to be included in the westernmost part of geophysical units B and A.

Unit "H2": represents the Punta Lara Facies defined by Cavallotto (1995, 1996), which is the basal part (sandy deposits, representing beaches environment) of Las Escobas Formation in the region, i.e. the late Holocene regressive sequence. In the PB transect this unit shows a prograding pattern

undoubtedly indicating regressive facies, and was also detected in the ED transect. This unit corresponds to the lithological units IV and III recognized in the short drillings.

Unit "H1": this is the typical beach ridges unit, named Cerro de la Gloria Facies by Cavallotto (1995, 1996) following the classical late Quaternary stratigraphy of the region. It is composed of two subunits: a) individual ridges (H1r) with an internal mounded structure that corresponds to lithological unit II, and b) inter-ridges (H1i) with an aggrading structure that corresponds to lithological unit I. In section ED, where ridges are evidenced in detail (Fig. 6), 22 individual ridges were detected, which are between 0.60 and 1 m high. Ridges spacing varies between 21 and 74 m averaging 44.2 m, although more than 70% of them are between 30 and 55 m. The crest of the individual ridges varies between 6 and 21 m wide, although in general they don´t exceed 15 m, with an average width of 10.6 m. In general, spacing between successive ridges (where inter-ridge deposits are present) increases as their crests become wider (Table 1).

Ridge N°	1 W	2	3	4	5	6	7	8	9	10	11	12	13	14	15	16	17	18	19	20	21	22 E
Crest width (m)		10	10	12	8	11	21	17	7	15	13	11	10	12	7	6	12	9	9	10	6	7
Spacing (m)	55	50	40	35	52	45	67	28	42	21	48	52	55	39	36	35	74	44	41	36	34	

Table 1: Geometric relations of the succession of individual ridges recognized in the subsoil by geophysical methods.

The geometry, spacing, ridges height and crests width of the subsoil ridges are equivalent to the geometry, spacing, ridges height and crests width of surface ridges observed in many places according to satellite images. It demonstrates that the employed geophysical methods are very good for discriminating these kind of geological structures and facies changes in the subsoil and for delineating their continuity, what will be very useful in regions where surface geological features don´t allow getting clues on the subsurface features.

8. Final remarks

We have investigated the shallow sedimentary structures of the southern coastal plain of the Río de La Plata in a continuous way by using geophysical methods and short drillings. This represents the first geophysical survey performed along a large transect that comprises the entire Holocene sequence in the region to study its stratigraphic characteristics. The structure and facies changes of the Holocene sedimentary sequences that compose the beach ridges system and associated environments of the investigated parts of the region were defined. Two major geophysical horizons were recognized which define three geophysical and stratigraphic units, one of Plio-Pleistocene age (of continental origin correlated with the "Pampean" deposits) and two of Holocene age (corresponding to the post-glacial transgressive-regressive deposits). In this way, the subsurface

extension of the Holocene sedimentary sequences could be established, which enhances the knowledge of the stratigraphy of this part of the region, only known until now by surface geology, outcrops and drillings. The relation between the Holocene sedimentary sequences and its substratum, as well as the distribution of beach ridges and the associated inter-ridges deposits were major results of the applied methodologies.

GPR produced good definition and resolution of the reflections of interest in most parts of the profiles. In some intervals of PB transect, the trajectories of the main reflections were ambiguous or insufficiently defined, so only tentative interpretations of them could be performed. In these intervals, ERT and MASW were useful to obtain complementary information about the subsoil that, after a joint interpretation of the geophysical results significantly reduced the GPR ambiguities. In this way, the integrated interpretation of the geophysical results increased the details, precision and robustness of the final interpretation.

Some problematic sections of the PB transect were found. In one of them (x = 1000 m), GRP showed weak, closely spaced and fluctuating reflections which were difficult to distinguish between them and track along the section. In another sector (x = 2000 m), the radargrams showed abundant and intense clutter produced by air reflections from the surrounding vegetation and a nearby power line, which almost completely masked the reflections of interest. In both cases, ERT and MASW determined well-defined resistivity and propagation velocity zones, respectively, whose boundaries agreed with the tentative GPR interpretation, thus reinforcing it. In the third problematic part of PB, the site where one of the main reflections reaches the surface could be established only very approximately from the GPR data, because the direct waves occupied a significant time-interval along the surface. In this case, the ERT method confirmed the outcrop of the reflector, and limited the interval of its position.

The sections investigated with the geophysical methods revealed the subsurface geological structure of the southern coastal plain of the Río de La Plata with larger details than were previously known. Then, the implemented methodology and resulting electromagnetic, electric and acoustic responses can be useful for future investigations of other sectors of this region, as well as in other sites with similar geological structure.

Acknowledgements

This research was supported by projects financed by the Agencia Nacional de Promoción Científica y Tecnológica (Argentina), PICT 2014/1613 and PICT 2017/1044. Authors deeply thank the editors of JSAES and reviewers for their valuable comments and suggestions that significantly improved the quality of this contribution.

References

Aguirre, M.L. and Whatley, R.C., 1995. Late Quaternary marginal marine deposits from north-eastern Buenos Aires Province, Argentina: a review. Quaternary Science Reviews 14: 223-254.

Aguirre, M.L., 1993. Palaeobiogeography of the Holocene molluscan fauna from Northeastern Buenos Aires Province, Argentina: its relation to coastal evolution and sea level changes. Palaeogeography, Palaeoclimatology, Palaeoecology 102: 1-26.

Ameghino, F., 1880. La Formación Pampeana o estudio sobre los terrenos de transporte de la Cuenca del Plata. G.Mason, París, 376 p.

Ameghino, F., 1908. Las formaciones sedimentarias de la región litoral de Mar del Plata y Chapalmalan. Anales Museo Nacional de Buenos Aires 10, 3ª. Sección: 343-428.

Bonomo, N., de la Vega, M., Martinelli, P. and Osella, A., 2011. Pipe-flange detection with GPR. Journal of Geophysics and Engineering 8: 35-45.

Bonomo, N., Osella, A., Martinelli, H., de la Vega, M., Cocco, G., Letieri, F. and Frittegotto, G., 2012. Location and characterization of the Sancti Spiritus Fort from geophysical investigations. Journal of Applied Geophysics 83: 57–64.

Cavallotto, J.L. and Violante, R. A., 2005. Geología y Geomorfología del Río de la Plata. 2005. In: de Barrio, R., Etcheverry, R. O., Caballé, M. F. y Llambías, E. (Eds.): Geología y recursos minerales de la Provincia de Buenos Aires. Relatorio XVI Congreso Geológico Argentino, La Plata XIV: 237-253.

Cavallotto, J.L., 1995. Evolución geomorfológica de la llanura costera ubicada en la margen sur del Río de la Plata. Tesis Doctoral Facultad de Ciencias Naturales y Museo, UNLP. 237 pp, 1 app. (Inédito).

Cavallotto, J.L., 1996. Estratigrafía del Holoceno de la Llanura costera del margen sur del Río de la Plata, XIII Congreso Geológico Argentino y III Congreso de Exploración de Hidrocarburos, Buenos Aires. Actas IV: 51-68.

Cavallotto, J.L., 2002. Evolución holocena de la llanura costera del margen sur del Río de la Plata. Revista Asociación Geológica Argentina 57 (4): 376-388.

Cavallotto, J.L., Violante, R.A and Colombo, F., 2005. Evolución y cambios ambientales de la llanura costera de la cabecera del Río de la Plata, Revista Asociación Geológica Argentina 60 (2): 353-367.

Cavallotto, J.L., Violante, R.A. and Parker, G., 2004. Sea level fluctuation during the last 8600 yrs in the Río de la Plata (Argentina). Quaternary International 114 (1): 155-165.

Cellone, F.A., Tosi, L. and Carol, E.S., 2018. Estimating the freshwater-lens reserve in the coastal plain of the middle Río de la Plata Estuary (Argentina). Science of the Total Environment 630 (7): 357-366.

Colombo, F., Rivero, L. and Casas, A., 2007. Contribución del georadar a la estratigrafía del delta del Río Paraná (Argentina): Primeros resultados. Geogaceta 41: 55-58.

Cox, R.B. and Teague, D.P., 2016. Layering ratios: a systematic approach to the inversion of surface wave data in the absence of a priori information. Geophysical Journal International 207: 422–438.

da Rocha, T.B., Fernandez, G.B. and Peixoto, M.N.O., 2013. Applications of ground-penetrating radar to investigate the Quaternary evolution of the south part of the Paraiba do Sul river delta (Rio de Janeiro, Brazil). Journal of Coastal Research 65 (sp1): 570-575.

Dahlin, T. and Zhou, B., 2004. A numerical comparison of 2D resistivity imaging with ten electrode arrays. Geophysical Prospecting 52: 379–98.

de la Vega, M., López, E., Osella, A., Rovere, E. and Violante, R.A., 2012. Quaternary volcanic-sedimentary sequences and evolution of the Llancanelo lake region (Southern Mendoza, Argentina) evidenced from geoelectric methods. Journal of South American Earth Science, 40, 116-128. DOI: 10.1016/j.jsames.2012.08.002

DeGroot-Hedlin, C. and Constable, S., 1990. Occam's inversion to generate smooth, two-dimensional models from magnetotelluric data. Geophysics 55: 1613–1624.

Doering, A., 1882. Geología. In: Informe de la Comisión Científica agregada al Estado Mayor General de la Expedición al Río Negro. Entrega III. Buenos Aires.

Dougherty, A.J., Choi, J-H, Turney, C.S.M. and Dosseto, A., 2019. Technical note: Optimizing the utility of combined GPR, OSL, and Lidar (GOaL) to extract paleoenvironmental records and decipher shoreline evolution. Climate of the Past (EGU) 15: 389–404.

Fidalgo, F., Colado, U. and De Francesco, F., 1973 a. Sobre ingresiones marinas cuaternarias en los partidos de Castelli, Chascomús y Magdalena (Provincia de Buenos Aires). 5º Congreso Geológico Argentino, Carlos Paz, Córdoba (1973), Actas 3: 227-240.

Fidalgo, F., De Francesco, F. and Colado, U., 1973 b. Geología superficial en las hojas Castelli, J.M. Cobo y Monasterio (Provincia de Buenos Aires). 5º Congreso Geológico Argentino, Carlos Paz, Córdoba (1973), Actas 4: 27-39.

Fidalgo, F., De Francesco, F. and Pascual, R., 1975. Geología superficial de la llanura bonaerense. En: Relatorio Geología de la Provincia de Buenos aires, VI Congreso Geológico Argentino, Bahía Blanca: 103-138.

Frenguelli, J., 1950. Rasgos generales de la morfología y la geología de la Prov. de Buenos Aires. LEMIT, MOP, La Plata, serie II (33): 72 p.

Frenguelli, J., 1957. Neozoico. In: Geografía de la República Argentina. GAEA 2, 3rd. Part: 1-113.

Fucks, E.E., Schnack E.J. and Aguirre M.L., 2010. Nuevo ordenamiento estratigráfico de las secuencias marinas del sector continental de la bahía Samborombón, provincia de Buenos Aires. Revista de la Asociación Geológica Argentina 67 (1): 27–39.

Jol H.M. (Ed.), 2009. Ground Penetrating Radar theory and applications. Elsevier Science, Amsterdam, 544 pp.

Leandro, C.G., Barboza, E.G., Caron, F. and de Jesus, F.A.N., 2019. GPR trace analysis for coastal depositional environments of southern Brazil. Journal of Applied Geophysics 162: 1-12.

Loke, M.H. and Barker, R.D., 1996. Rapid least-squares inversion of apparent resistivity pseudosections by quasi Nexton method. Geophysical Prospecting 44: 131–52.

Martorana, R., Fiandaca, G., Casas Ponsati, A. and Cosentino, P.L., 2009. Comparative tests on different multi-electrode arrays using models in near-surface geophysics. Journal of Geophysics and Engineering 6: 1–20.

O'Neal, M.L. and Dunn, R.K., 2015. GPR investigation of multiple stage-5 sea-level fluctuations on a siliciclastic estuarine shoreline, Delaware Bay, southern New Jersey, USA. In: Bristow, C.S. and Jol, H.M. (Eds.), Ground Penetrating Radar in Sediments. Geological Society, London, Special Publication 211: 67-77.

Onnis, L.E., Osella, A. and Carcione, J.M., 2019. Retrieving shallow shear-wave velocity profiles from 2D seismic-reflection data with severely aliased surface waves. Journal of Applied Geophysics 161: 25-35. https://doi.org/10.1016/j.jappgeo.2018.11.014

Parker, G. and Violante, R.A., 1993. Río de la Plata y regiones adyacentes. In: Iriondo, M. (Ed.): El Holoceno en la Argentina 2: 163-229, CADINQUA-AGA-CONICET.

Parker, G., Paterlini, C.M. and Violante, R.A., 1994. Edad y génesis del Río de la Plata. Revista de la Asociación Geológica Argentina 49 (1-2): 11-18.

Paz, C., Alcalá, F.J., Carvalho, J.M. and Ribeiro, L., 2017. Current uses of ground penetrating radar in groundwater-dependent ecosystems research, Science of the Total Environment, 595: 868-885.

Perdomo, S., Ainchil, J.E. and Kruse E., 2014 a. Hydraulic parameters estimation from well logging resistivity and geoelectrical measurements. Journal of Applied Geophysics 105: 50-58.

Perdomo, S., Kruse E. and Ainchil, J.E., 2014 b. Estimation of hydraulic parameters using electrical resistivity tomography (ERT) and empirical laws in a semi-confined aquifer. Near Surface Geophysics, 16: 627-641.

Pipan, M., Forte, E., Dal Moro, G., Sugan, M. and Finetti, I., 2017. Multifold ground-penetrating radar and resistivity to study the stratigraphy of shallow unconsolidated sediments, The Leading Edge 22 (9): 801-920.

Prieto, A.R., Mourelle C.D., Peltier, W.R., Drummond, R., Vilanova, I. and Ricci, L., 2016. Relative sea-level changes during the Holocene in the Río de la Plata, Argentina and Uruguay: A review. Quaternary International 442: 35-49.

Richiano, S., Varela, A.N., D´Elia, L., Bilmes, A. and Aguirre M.L., 2012. Evolución paleoambiental de cordones litorales holocenos durante una caída del nivel del mar en la Bahía Samborombón, Buenos Aires, Argentina. Latin American Journal of Sedimentology and Basin Analysis 19 (2): 105-124.

Sambridge, M., 1999. Geophysical inversion with a neighbourhood algorithm - I. Searching a parameter space. Geophysical Journal International 138: 479–494. https://doi.org/10.1046/j.1365-246X.1999.00876.x.

Schwenk, J., Sloan, S., Ivanov, J. and Miller R. D., 2016. Surface-wave methods for anomaly detection. Geophysics, 81 (4), EN29-EN42, doi:10.1190/geo2015-0356.1.

Szalai, S., Novák, A. and Szarka, L., 2011. Which geoelectric array sees the deepest in a noisy environment? Depth of detectability values of multielectrode systems for various 2D models. Journal of Physics and Chemistry of the Earth 36: 1398–1404.

Tillmann, T. and Wunderlich, J., 2012. Ground-penetrating radar in coastal environments: examples from the islands Sylt and Amrum. Bremer Beiträge zur Geographie u. Raumplanung 44: 60-77.

Van Heteren, S. and Fitzgerald, D., 2017. Application of ground-penetreting radar in coastal stratigraphic studies. En: Finkl, C.W. and Makowski, C. (Eds.), Encyclopedia of Coastal Science, Springer International, DOI 10.1007/978-3-319-48657-4_162-2.

Wathelet, M., 2008. An improved neighborhood algorithm: Parameter conditions and dynamic scaling. Geophysical Research Letters 35. https://doi.org/10.1029/2008GL033256.

Yin, Y., Zhu, D., Tang, W. and Martini, I.P., 2002. The application of GPR to barrier-lagoon sedimentation study in Boao of Hainan Island. Journal of Geographical Sciences 12 (3): 313-320.

Zabala Medina, P., Limarino, C., Bonomo, N., Salvó Bernárdez, S. and Osella, A., 2020. Using Ground Penetrating Radar and attribute analysis for identifying depositional units in a fluvial-aeolian interaction environment: The Guandacol Valley, northwest Argentina. Journal of South American Earth Sciences 98: 1-16.

Highlights

First geophysical survey through the beach ridges coastal plain of the Province of Buenos Aires, with stratigraphic objectives.

First work combining diverse geophysical technics in the region.

Authors statement

All the authors and coauthors agree with the content of the manuscript and have contributed to it.

Cavallotto, J.L .
Bonomo, N.
Grunhut, V.
Zabala Medina, P.
Violante, R.A.
Onnis, L.
Osella, A.

Declaration of interests

The authors declare that they have no known competing financial interests or personal relationships that could have appeared to influence the work reported in this paper.